Appl. Math. Mech. -Engl. Ed., **38**(9), 1273–1294 (2017)
DOI 10.1007/s10483-017-2237-8

Applied Mathematics and Mechanics (English Edition)

Analytical method for evaluating stress field in casing-cement-formation system of oil/gas wells*

Wei LIU†, Baohua YU, Jingen DENG

State Key Laboratory of Petroleum Resources and Prospecting,
China University of Petroleum, Beijing 102249, China

Abstract In this paper, we present an analytical method for evaluating the stress field within a casing-cement-formation system of oil/gas wells under anisotropic in-situ stresses in the rock formation and uniform pressure within the casing. The present method treats the in-situ stresses in the formation as initial stresses since the in-situ stresses have already developed in the formation before placement of cement and casing into the well. It is demonstrated that, via this treatment, the present method excludes additional displacements within the formation predicted by the existing method, and gives more reasonable stress results. An actual tight-oil well is analyzed using the present and existing analytical methods, as well as the finite element method. Good agreement between the analytical results and the finite element analysis (FEA) results is obtained, validating the present method. It is also evident that, compared with the present method, the existing method overestimates the compressive stress level within the casing and the cement. Finally, the effects of elastic properties of the formation, cement, and inner pressure of casing on stresses within the casing and cement are illustrated with a series of sensitivity analyses.

Key words near wellbore region, stress evaluation, anisotropic in-situ stress, initial stress

Chinese Library Classification O343.1
2010 Mathematics Subject Classification 74B10, 74G05

1 Introduction

The increasingly complex environment in which oil and natural gas wells operate has imposed more and more critical design constraints on the well drilling and completion. For example, more and more high pressure/high temperature wells, deep and ultra-deep wells and massively hydraulically fractured horizontal wells are drilled, which brings about extreme conditions like the high temperature, high pore pressure, high in-situ stress as well as high internal pressure within the steel casing. Therefore, wellbore integrity has always been a central concern during the design of wells exposed to these harsh conditions. Among various well integrity issues, mechanical failures of the steel casing and the cement sheath are two primary failure

* Received Sept. 2, 2016 / Revised Jan. 25, 2017
Project supported by the National Natural Science Foundation of China (Nos. 11502304 and 51521063) and the Science Foundation of China University of Petroleum (Nos. C201601 and 2462013YJRC023)
† Corresponding author, E-mail: liuwei@cup.edu.cn

types[1]. Experimental and field experiences showed that mechanical failures of the casing and the cement could occur due to excessive stresses induced by dramatic changes of down-hole conditions during operations such as hydraulic fracturing, hot fluid/steam injection, well testing and production[2–3]. More critically, the mechanical failure may also incur or speed up chemical degradation of the casing and the cement due to corrosive substances in the reservoir fluids, thus accelerating the mechanical failure[4–5]. The failure of the casing may lead to compromised oil/gas production and even abandonment of the well, while the failure of the cement would cause loss of effective zonal isolation and uncontrolled leakage of oil/gas from the reservoir to shallow aquifers, leading to environmental and safety concerns[6–7]. Thus, in order to ensure the integrity of the casing and the cement by appropriate design, it is of paramount importance to accurately evaluate stresses within the casing and the cement during the whole operating life circle of the well.

Laboratory investigations simulating down-hole conditions[2,8] have been conducted to understand the mechanical behavior of the cement sheath, which manifested that radial tensile cracking and compressive or shear plastic damaging may occur within the cement depending on the stress conditions, and also demonstrated the significant influence of the mechanical properties of the casing, the cement, and the formation. Meanwhile, the industry has acknowledged from field experiences that there is a positive effect of the cement on the failure resistance of the casing[9]. These facts suggest that the stress field within the near wellbore region depends on the interactions among the casing, the cement, and the formation, which justifies the need of determining the stresses in the three components as a whole system.

Due to its versatility in tackling complex geometries and material behaviors, numerical modeling, especially the finite element modeling, has been widely used to determine the stresses within the near wellbore region and evaluate the integrity of the casing and the cement[5,9–17]. The simple two-dimensional elastic finite element analysis (FEA) was used to determine the stresses within cemented wellbores[5,9–12], which demonstrated the significant effects of mechanical properties of the cement and the formation on the stress conditions within the casing and the cement. More elaborated models have also been used to account for more sophisticated effects such as shrinkage or expansion of the cement, elastoplastic failure of the cement and the formation rock, as well as possible debonding of the casing-cement and cement-formation interfaces[13–17]. Three-dimensional finite element models were used to consider more complex details like heterogeneity of the rock formation along the depth[18].

In parallel with the numerical modeling works, analytical methods have been developed and used to calculate stresses within the casing-cement-formation system. Aiming at determining the directions of hydraulic fractures, Atkinson and Eftaxiopoulos[19] presented a plane model for the stress field around the cased and cemented wellbore, which was recently used by Yuan et al.[20] to calculate the stresses within the cement sheath of water-injection wells. Thiercelin et al.[21] developed an analytical model for evaluating the stresses in a casing-cement-formation system due to variations of inner pressure of casing. Yin et al.[22] gave a comprehensively analytical solution of the stress distribution in a casing-cement-formation system under anisotropic in-situ stresses. Li et al.[23] theoretically analyzed the stresses within the cement subjected to anisotropic in-situ stresses and uniform inner pressures of casing. Similar analytical works with the temperature effect taken into account have also emerged[5,24–25]. In all these models, the casing-cement and cement-formation interfaces are taken as fully bonded. Recently, Zhang et al.[26] developed an analytical model in which the two interfaces were explicitly considered as extremely thin layers of homogeneous isotropic materials, and gave stresses within the five-layered casing-interface-cement-interface-formation system under anisotropic in-situ stresses as well as temperature variations.

By examining the above existing analytical methods, it is not hard to find that in-situ stresses in the formation, either isotropic or anisotropic, have been utilized only as stress boundary conditions at the outer boundary of the formation. We suggest here that this treatment

would be inaccurate, because this would predict unrealistic additional displacements within the formation, as demonstrated later in this paper. Since the final solution is constructed with the conditions that displacements and tractions are continuous across the casing-cement and cement-formation interfaces, additional displacements within the formation would affect the stress distribution and bring about inaccuracy in the final solution. Thus, in this paper, we propose a revised analytical method for stress evaluation within the casing-cement-formation system, in which the in-situ stresses are taken not only as stress boundary conditions at the outer boundary of the formation but also as initial stresses in the constitutive law of the formation. In this way, the additional displacements within the formation predicted by the existing method can be excluded, and the resulting stress solution can be more accurate.

The paper is organized as follows. In Section 2, we will firstly present the problem description and decomposition as well as some basic equations, which are followed by detailed derivations of the revised analytical method, and then some remarks on the significance of the present analytical method and the differences between the present method and the existing method will be given. Section 3 offers a validation of the present analytical method and results of a series of sensitivity analyses. Finally, in Section 4, some conclusions are drawn.

2 Revised analytical method

2.1 Problem description, decomposition and basic equations

After drilling and completion, the near wellbore region of the production interval of oil/gas wells is generally composed of three components: steel casing, cement sheath, and rock formation. Figure 1(a) is a sketch of a typical cross-section of the casing-cement-formation system, where Ω^1, Ω^2 and Ω^3 represent the steel casing, the cement sheath, and the rock formation, respectively. The inner radii of the casing, the cement, and the formation are r_1, r_2, and r_3, respectively. Before the well construction, in-situ compressive stresses develop in the formation during the sedimentary process and the tectonic process. The in-situ stress state of the formation is generally characterized by its three principal stresses, one of which is in the vertical direction, denoted as σ_{V}, and the other two, generally unequal, are in horizontal directions, with the larger one denoted as σ_{H} and the smaller one σ_{h}. A uniform wellbore pressure p_{w} acts on the inner surface of the casing, which results from the weight of the fluid within the casing, e.g., the drilling fluid or the hydraulic fracturing fluid. The objective is to determine the stress field within the casing-cement-formation system. This problem is three-dimensional in nature. However, possible axial deformations of the casing, cement, and formation are generally limited compared with the depth of oil/gas wells, especially at positions far away from the wellhead. Thus, it could be an appropriate approximation to treat the problem as a plane strain problem, as exercised in previous literatures[21–22,25–26].

A Cartesian coordinate system is set up and shown in Fig. 1 with x-, y-, and z-directions in accord with the σ_{H}-, σ_{h}-, and σ_{V}-directions, respectively. In this coordinate system, the in-situ stresses within the formation can be written as

$$\sigma_{xx} = -\sigma_{\mathrm{H}}, \quad \sigma_{yy} = -\sigma_{\mathrm{h}}. \tag{1}$$

Since the casing and the cement are hollow circular cylinders, and the formation can also be taken as a hollow circular cylinder with an infinite outer radius, it is convenient to solve the problem in a polar coordinate system. Thus, the in-situ stresses within the rock formation can be rewritten as follows:

$$\sigma_r = -\sigma - s\cos(2\theta), \quad \sigma_\theta = -\sigma + s\cos(2\theta), \quad \tau_{r\theta} = s\sin(2\theta), \tag{2}$$

where θ is the polar angle measured from the x-direction, i.e., from the σ_{H}-direction, and

$$\sigma = \frac{1}{2}(\sigma_{\mathrm{H}} + \sigma_{\mathrm{h}}), \quad s = \frac{1}{2}(\sigma_{\mathrm{H}} - \sigma_{\mathrm{h}}).$$

In this study, the casing, the cement sheath, and the formation are assumed to be of homogeneous, isotropic, and linearly elastic materials. The stress distribution within the composite system will be calculated in the framework of theory of elasticity, and thus the superposition principle holds, justifying a decomposition of the complete problem in Fig. 1(a) into two sub-problems, as shown in Figs. 1(b) and 1(c).

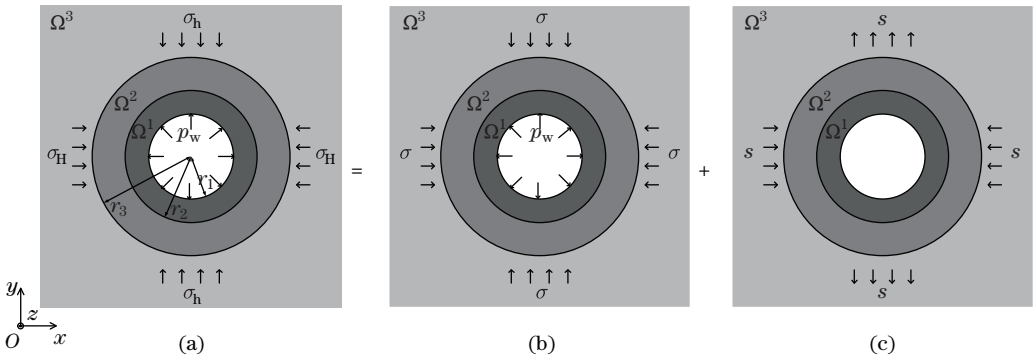

Fig. 1 Sketches of casing-cement-formation system under (a) anisotropic horizontal in-situ stresses, (b) isotropic horizontal in-situ stresses, and (c) deviatoric horizontal in-situ stresses

Sub-problem I As shown in Fig. 1(b), an isotropic in-situ stress σ exists in the formation, and a uniform pressure p_w is applied on the casing inner surface. The stress conditions in the formation can be written as

$$\sigma_r = -\sigma, \quad \tau_{r\theta} = 0, \tag{3}$$

and at the inner surface of the casing,

$$\sigma_r = -p_w, \quad \tau_{r\theta} = 0. \tag{4}$$

Sub-problem II As shown in Fig. 1(c), a deviatoric in-situ stress s exists in the formation, and the casing inner surface is traction-free. In this case, the stress conditions in the formation can be expressed as

$$\sigma_r = -s\cos(2\theta), \quad \sigma_\theta = s\cos(2\theta), \quad \tau_{r\theta} = s\sin(2\theta), \tag{5}$$

and at the inner surface of the casing, the stress boundary conditions are

$$\sigma_r = 0, \quad \tau_{r\theta} = 0. \tag{6}$$

In the following three subsections, solutions of Sub-problem I and Sub-problem II will be given separately and then combined to give the solution of the complete problem, i.e., the stress distribution within the casing-cement-formation system. Before proceeding to give the specific results, some basic equations are presented here for completeness. For a plane strain problem, in the absence of body force, the equilibrium equations take the following form in a polar coordinate system[27]:

$$\begin{cases} \dfrac{\partial \sigma_r}{\partial r} + \dfrac{1}{r}\dfrac{\partial \tau_{r\theta}}{\partial \theta} + \dfrac{\sigma_r - \sigma_\theta}{r} = 0, \\ \dfrac{\partial \tau_{r\theta}}{\partial r} + \dfrac{1}{r}\dfrac{\partial \sigma_\theta}{\partial \theta} + \dfrac{2\tau_{r\theta}}{r} = 0. \end{cases} \tag{7}$$

The infinitesimal strain-displacement relationship can be expressed as[27]

$$\varepsilon_r = \frac{\partial u_r}{\partial r}, \quad \varepsilon_\theta = \frac{1}{r}\frac{\partial u_\theta}{\partial \theta} + \frac{u_r}{r}, \quad \gamma_{r\theta} = \frac{\partial u_\theta}{\partial r} + \frac{1}{r}\frac{\partial u_r}{\partial \theta} - \frac{u_\theta}{r}. \tag{8}$$

Hooke's law with initial stresses considered reads

$$\begin{cases} \varepsilon_r = \dfrac{1+\upsilon}{E}((1-\upsilon)(\sigma_r-\sigma_r^0)-\upsilon(\sigma_\theta-\sigma_\theta^0)), \\ \varepsilon_\theta = \dfrac{1+\upsilon}{E}((1-\upsilon)(\sigma_\theta-\sigma_\theta^0)-\upsilon(\sigma_r-\sigma_r^0)), \\ \gamma_{r\theta} = \dfrac{2(1+\upsilon)}{E}(\tau_{r\theta}-\tau_{r\theta}^0), \end{cases} \tag{9}$$

where E is Young's modulus, υ is Poisson's ratio, and σ_r^0, σ_θ^0, and $\tau_{r\theta}^0$ are the initial radial, hoop, and shear stress components, respectively.

Using the concept of stress function, the compatibility equation is in the following form[27]:

$$\Big(\frac{\partial^2}{\partial r^2}+\frac{1}{r}\frac{\partial}{\partial r}+\frac{1}{r^2}\frac{\partial^2}{\partial\theta^2}\Big)\Big(\frac{\partial^2\varphi}{\partial r^2}+\frac{1}{r}\frac{\partial\varphi}{\partial r}+\frac{1}{r^2}\frac{\partial^2\varphi}{\partial\theta^2}\Big)=0, \tag{10}$$

where φ is the stress function, and the stress components can be related to the stress function in the following manner[27]:

$$\sigma_r=\frac{1}{r}\frac{\partial\varphi}{\partial r}+\frac{1}{r^2}\frac{\partial^2\varphi}{\partial\theta^2},\quad \sigma_\theta=\frac{\partial^2\varphi}{\partial r^2},\quad \tau_{r\theta}=-\frac{\partial}{\partial r}\Big(\frac{1}{r}\frac{\partial\varphi}{\partial\theta}\Big). \tag{11}$$

2.2 Solution of Sub-problem I

For Sub-problem I shown in Fig. 1(b), the configuration is axisymmetric. Therefore, the casing, the cement, and the formation could be taken as hollow cylinders submitted to uniform pressures on the inner and outer surfaces, as shown in the subfigure (a) of Fig. 2, where r_i and r_o denote the inner and outer radii of the cylinder, σ_i and σ_o are the uniform internal and external pressures, and s_i and s_o are the normal stresses at the internal surface and external surface, respectively.

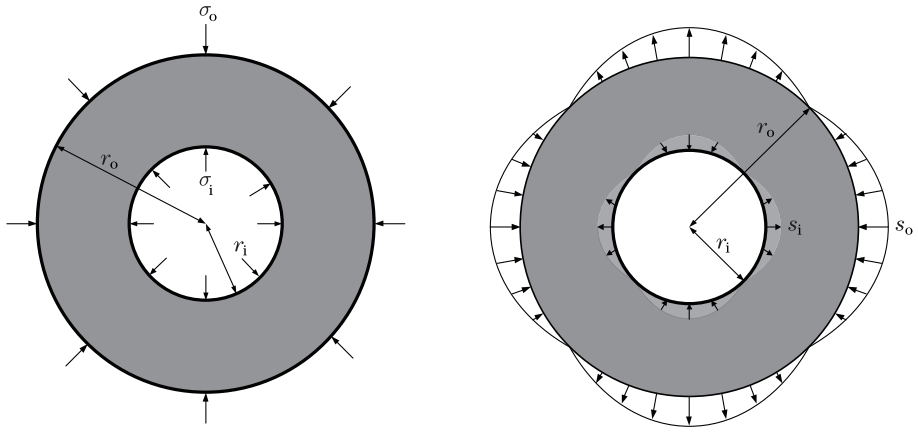

(a) (b)

Fig. 2 (a) Hollow cylinder submitted to uniform pressures at inner and outer surfaces, representing any one of three components, i.e., casing, cement, and formation in Sub-problem I; (b) hollow cylinder representative of any one of three components in Sub-problem II, under application of normal and shear tractions varying with angle θ in cosinoidal and sinusoidal fashions

The general solutions of the stress distribution are obtained as[27]

$$\begin{cases} \sigma_r = \dfrac{r_\mathrm{i}^2\sigma_\mathrm{i}-r_\mathrm{o}^2\sigma_\mathrm{o}}{r_\mathrm{o}^2-r_\mathrm{i}^2}+\dfrac{r_\mathrm{i}^2r_\mathrm{o}^2(\sigma_\mathrm{o}-\sigma_\mathrm{i})}{r_\mathrm{o}^2-r_\mathrm{i}^2}\dfrac{1}{r^2}, \\ \sigma_\theta = \dfrac{r_\mathrm{i}^2\sigma_\mathrm{i}-r_\mathrm{o}^2\sigma_\mathrm{o}}{r_\mathrm{o}^2-r_\mathrm{i}^2}-\dfrac{r_\mathrm{i}^2r_\mathrm{o}^2(\sigma_\mathrm{o}-\sigma_\mathrm{i})}{r_\mathrm{o}^2-r_\mathrm{i}^2}\dfrac{1}{r^2}. \end{cases} \tag{12}$$

Substituting these two stress components into Hooke's law in Eq. (9) yields the hoop strain ε_θ. Then, by using the second expression of Eq. (8) where the first term on the right hand side is zero due to the axial symmetry of Sub-problem I, we obtain the following general solution of the radial displacement with initial stresses considered:

$$u_r = \frac{(1+\upsilon)r}{E}\Big((1-2\upsilon)\frac{r_{\rm i}^2\sigma_{\rm i} - r_{\rm o}^2\sigma_{\rm o}}{r_{\rm o}^2 - r_{\rm i}^2} + \frac{r_{\rm i}^2 r_{\rm o}^2(\sigma_{\rm i} - \sigma_{\rm o})}{r_{\rm o}^2 - r_{\rm i}^2}\frac{1}{r^2} - (1-\upsilon)\sigma_\theta^0 + \upsilon\sigma_r^0\Big). \tag{13}$$

Equation (13) can be rearranged as follows:

$$u_r = \frac{r_{\rm i}^2\sigma_{\rm i} - r_{\rm o}^2\sigma_{\rm o}}{\alpha(r_{\rm o}^2 - r_{\rm i}^2)}r + \frac{r_{\rm i}^2 r_{\rm o}^2(\sigma_{\rm i} - \sigma_{\rm o})}{\beta(r_{\rm o}^2 - r_{\rm i}^2)}\frac{1}{r} + \frac{\upsilon\sigma_r^0 - (1-\upsilon)\sigma_\theta^0}{\beta}r, \tag{14}$$

where the two parameters α and β are defined as

$$\alpha = \frac{E}{(1+\upsilon)(1-2\upsilon)}, \quad \beta = \frac{E}{(1+\upsilon)}. \tag{15}$$

Assume that the casing-cement and the cement-formation interfaces are perfect, which indicates that the tractions and displacements are continuous crossing these interfaces. Due to the axial symmetry of Sub-problem I, only the radial traction and displacement are presented. Let p_2 and p_3 denote contact pressures at the casing-cement and cement-formation interfaces, respectively. For the casing, we have

$$\sigma_\theta^0 = \sigma_r^0 = 0, \quad r_{\rm i} = r_1, \quad r_{\rm o} = r_2, \quad \sigma_{\rm i} = p_{\rm w}, \quad \sigma_{\rm o} = p_2. \tag{16}$$

Thus, from Eq. (14), the radial displacement field within the casing is

$$u_r^1 = \frac{r_1^2 p_{\rm w} - r_2^2 p_2}{\alpha_1(r_2^2 - r_1^2)}r + \frac{r_1^2 r_2^2(p_{\rm w} - p_2)}{\beta_1(r_2^2 - r_1^2)}\frac{1}{r}, \tag{17}$$

where α_1 and β_1 have been defined in Eq. (15), and the subscript 1 signifies that these parameters are for the casing.

For the cement sheath, we have

$$\sigma_\theta^0 = \sigma_r^0 = 0, \quad r_{\rm i} = r_2, \quad r_{\rm o} = r_3, \quad \sigma_{\rm i} = p_2, \quad \sigma_{\rm o} = p_3. \tag{18}$$

Similarly, from Eq. (14), the radial displacement field within the cement is obtained as

$$u_r^2 = \frac{r_2^2 p_2 - r_3^2 p_3}{\alpha_2(r_3^2 - r_2^2)}r + \frac{r_2^2 r_3^2(p_2 - p_3)}{\beta_2(r_3^2 - r_2^2)}\frac{1}{r}. \tag{19}$$

For the formation, we have

$$\sigma_\theta^0 = \sigma_r^0 = -\sigma, \quad r_{\rm i} = r_3, \quad r_{\rm o} = \infty, \quad \sigma_{\rm i} = p_3, \quad \sigma_{\rm o} = \sigma. \tag{20}$$

Substitution of Eq. (20) into Eq. (14) yields the following radial displacement field for the formation:

$$u_r^3 = \frac{r_3^2(p_3 - \sigma)}{\beta_3}\frac{1}{r}. \tag{21}$$

The normal traction continuity conditions at the casing-cement interface and the cement-formation interface have been implicitly enforced by assigning a contact pressure at each of these two surfaces. Moreover, continuity of radial displacements at the two interfaces gives

$$u_r^1\big|_{r=r_2} = u_r^2\big|_{r=r_2}, \quad u_r^2\big|_{r=r_3} = u_r^3\big|_{r=r_3}. \tag{22}$$

Substituting Eqs. (17), (19), and (21) into Eq. (22), we obtain

$$\begin{cases} \dfrac{r_1^2 p_{\mathrm{w}} - r_2^2 p_2}{\alpha_1(r_2^2 - r_1^2)} r_2 + \dfrac{r_1^2 r_2^2 (p_{\mathrm{w}} - p_2)}{\beta_1(r_2^2 - r_1^2)} \dfrac{1}{r_2} = \dfrac{r_2^2 p_2 - r_3^2 p_3}{\alpha_2(r_3^2 - r_2^2)} r_2 + \dfrac{r_2^2 r_3^2 (p_2 - p_3)}{\beta_2(r_3^2 - r_2^2)} \dfrac{1}{r_2}, \\ \dfrac{r_2^2 p_2 - r_3^2 p_3}{\alpha_2(r_3^2 - r_2^2)} r_3 + \dfrac{r_2^2 r_3^2 (p_2 - p_3)}{\beta_2(r_3^2 - r_2^2)} \dfrac{1}{r_3} = \dfrac{r_3^2 (p_3 - \sigma)}{\beta_3} \dfrac{1}{r_3}. \end{cases} \tag{23}$$

Equation (23) can be rearranged as

$$\begin{cases} \Big(\dfrac{\alpha_1 r_1^2 + \beta_1 r_2^2}{\alpha_1 \beta_1 (r_2^2 - r_1^2)} + \dfrac{\alpha_2 r_3^2 + \beta_2 r_2^2}{\alpha_2 \beta_2 (r_3^2 - r_2^2)} \Big) p_2 - \dfrac{(\alpha_2 + \beta_2) r_3^2}{\alpha_2 \beta_2 (r_3^2 - r_2^2)} p_3 = \dfrac{(\alpha_1 + \beta_1) r_1^2}{\alpha_1 \beta_1 (r_2^2 - r_1^2)} p_{\mathrm{w}}, \\ -\dfrac{(\alpha_2 + \beta_2) r_2^2}{\alpha_2 \beta_2 (r_3^2 - r_2^2)} p_2 + \Big(\dfrac{\alpha_2 r_2^2 + \beta_2 r_3^2}{\alpha_2 \beta_2 (r_3^2 - r_2^2)} + \dfrac{1}{\beta_3} \Big) p_3 = \dfrac{1}{\beta_3} \sigma, \end{cases} \tag{24}$$

which can be further rewritten in the following compact matrix form:

$$\begin{cases} A_{11} p_2 + A_{12} p_3 = B_1, \\ A_{21} p_2 + A_{22} p_3 = B_2, \end{cases} \tag{25}$$

where

$$A_{11} = \frac{\alpha_1 r_1^2 + \beta_1 r_2^2}{\alpha_1 \beta_1 (r_2^2 - r_1^2)} + \frac{\alpha_2 r_3^2 + \beta_2 r_2^2}{\alpha_2 \beta_2 (r_3^2 - r_2^2)}, \quad A_{12} = -\frac{(\alpha_2 + \beta_2) r_3^2}{\alpha_2 \beta_2 (r_3^2 - r_2^2)},$$

$$A_{21} = -\frac{(\alpha_2 + \beta_2) r_2^2}{\alpha_2 \beta_2 (r_3^2 - r_2^2)}, \quad A_{22} = \frac{\alpha_2 r_2^2 + \beta_2 r_3^2}{\alpha_2 \beta_2 (r_3^2 - r_2^2)} + \frac{1}{\beta_3},$$

$$B_1 = \frac{(\alpha_1 + \beta_1) r_1^2}{\alpha_1 \beta_1 (r_2^2 - r_1^2)} p_{\mathrm{w}}, \quad B_2 = \frac{\sigma}{\beta_3}.$$

From Eq. (25), the contact pressures p_2 and p_3 can be solved,

$$\begin{cases} p_2 = \dfrac{A_{22} B_1 - A_{12} B_2}{A_{11} A_{22} - A_{12} A_{21}}, \\ p_3 = \dfrac{A_{11} B_2 - A_{21} B_1}{A_{11} A_{22} - A_{12} A_{21}}. \end{cases} \tag{26}$$

Substitution of p_2 and p_3 back into Eqs. (12), (17), (19), and (21) yields the stress and displacement distributions within the casing-cement-formation system as the solution of Sub-problem I.

2.3 Solution of Sub-problem II

For Sub-problem II shown in Fig. 1(c), the in-situ stresses in the formation vary with the polar angle θ in cosinoidal and sinusoidal fashions, as shown in Eq. (5). The zero surface traction at the casing inner surface can also be taken as a particular form of cosinoidal or sinusoidal distribution with the zero amplitude. In this case, the casing, the cement, and the formation can be treated as hollow cylinders subjected to cosinoidal or sinusoidal distributions of normal and shear tractions at the inner and outer surfaces, as sketched in Fig. 2(b). The stress function for this type of problem is in the following general form[27]:

$$\varphi(r, \theta) = f(r) \cos(2\theta). \tag{27}$$

Substitution of Eq. (27) into the compatibility equation (10) yields the following forth-order ordinary differential equation:

$$\Big(\frac{\mathrm{d}^2}{\mathrm{d}r^2} + \frac{1}{r} \frac{\mathrm{d}}{\mathrm{d}r} - \frac{4}{r^2} \Big) \Big(\frac{\mathrm{d}^2 f}{\mathrm{d}r^2} + \frac{1}{r} \frac{\mathrm{d}f}{\mathrm{d}r} - \frac{4f}{r^2} \Big) = 0, \tag{28}$$

of which the general solution is

$$f(r) = Ar^4 + Br^2 + C + \frac{D}{r^2}. \tag{29}$$

The stress function is therefore given in the following form:

$$\varphi(r,\theta) = f(r)\cos(2\theta) = \Big(Ar^4 + Br^2 + C + \frac{D}{r^2}\Big)\cos(2\theta). \tag{30}$$

And from Eq. (11), the stress components are obtained as

$$\begin{cases} \sigma_r = -\Big(2B + \dfrac{4C}{r^2} + \dfrac{6D}{r^4}\Big)\cos(2\theta), \\ \sigma_\theta = \Big(12Ar^2 + 2B + \dfrac{6D}{r^4}\Big)\cos(2\theta), \\ \tau_{r\theta} = \Big(6Ar^2 + 2B - \dfrac{2C}{r^2} - \dfrac{6D}{r^4}\Big)\sin(2\theta). \end{cases} \tag{31}$$

Substituting the three stress components in Eq. (31) into Hooke's law in Eq. (9), we obtain

$$\begin{cases} \varepsilon_r = -\dfrac{1+\upsilon}{E}\Big(12\upsilon Ar^2 + 2B + (1-\upsilon)\dfrac{4C}{r^2} + \dfrac{6D}{r^4}\Big)\cos(2\theta) - \varepsilon_r^0, \\ \varepsilon_\theta = \dfrac{1+\upsilon}{E}\Big(12(1-\upsilon)Ar^2 + 2B + \upsilon\dfrac{4C}{r^2} + \dfrac{6D}{r^4}\Big)\cos(2\theta) - \varepsilon_\theta^0, \end{cases} \tag{32}$$

where

$$\begin{cases} \varepsilon_r^0 = \dfrac{1+\upsilon}{E}((1-\upsilon)\sigma_r^0 - \upsilon\sigma_\theta^0), \\ \varepsilon_\theta^0 = \dfrac{1+\upsilon}{E}((1-\upsilon)\sigma_\theta^0 - \upsilon\sigma_r^0). \end{cases} \tag{33}$$

Integration of the strain components in Eq. (32) gives the following general displacement solutions for each component of the casing-cement-formation system:

$$\begin{cases} u_r = -\dfrac{1+\upsilon}{E}\Big(4\upsilon Ar^3 + 2Br - (1-\upsilon)\dfrac{4C}{r} - \dfrac{2D}{r^3}\Big)\cos(2\theta) - r\varepsilon_r^0, \\ u_\theta = \dfrac{1+\upsilon}{2E}\Big(4(3-2\upsilon)Ar^3 + 4Br - (1-2\upsilon)\dfrac{4C}{r} + \dfrac{4D}{r^3}\Big)\sin(2\theta) + r\displaystyle\int(\varepsilon_r^0 - \varepsilon_\theta^0)\mathrm{d}\theta, \end{cases} \tag{34}$$

where rigid body motions are neglected.

For the casing and the cement,

$$\sigma_\theta^0 = \sigma_r^0 = 0, \quad \varepsilon_r^0 = \varepsilon_\theta^0 = 0. \tag{35}$$

Thus, the displacement field for the casing and cement is

$$\begin{cases} u_r^i = -\dfrac{1+\upsilon_i}{E_i}\Big(4\upsilon_i A_i r^3 + 2B_i r - (1-\upsilon_i)\dfrac{4C_i}{r} - \dfrac{2D_i}{r^3}\Big)\cos(2\theta), \\ u_\theta^i = \dfrac{1+\upsilon_i}{2E_i}\Big(4(3-2\upsilon_i)A_i r^3 + 4B_i r - (1-2\upsilon_i)\dfrac{4C_i}{r} + \dfrac{4D_i}{r^3}\Big)\sin(2\theta), \end{cases} \tag{36}$$

where $i = 1$ stands for the casing, and $i = 2$ refers to the cement.

For the formation, the stress conditions are

$$\sigma_r^0 = -\sigma_\theta^0 = -s\cos(2\theta), \quad \sigma_r|_{r=\infty} = -s\cos(2\theta), \quad \tau_{r\theta}|_{r=\infty} = s\sin(2\theta). \tag{37}$$

Substituting Eq. (31) into Eq. (37), we obtain

$$A_3 = 0, \quad B_3 = \frac{s}{2}. \tag{38}$$

And the displacement field for the formation can be obtained from Eqs. (32)–(34), (37) and (38) as

$$\begin{cases} u_r^3 = -\dfrac{1+\upsilon_3}{E_3}\Big(-(1-\upsilon_3)\dfrac{4C_3}{r} - \dfrac{2D_3}{r^3}\Big)\cos(2\theta), \\ u_\theta^3 = \dfrac{1+\upsilon_3}{2E_3}\Big(-(1-2\upsilon_3)\dfrac{4C_3}{r} + \dfrac{4D_3}{r^3}\Big)\sin(2\theta). \end{cases} \tag{39}$$

Again, we consider that the casing-cement interface and the cement-formation interface are perfect. Continuity of the tractions and the displacements at the interfaces gives

$$\begin{cases} \sigma_r^1|_{r=r_2} = \sigma_r^2|_{r=r_2}, \quad \tau_{r\theta}^1|_{r=r_2} = \tau_{r\theta}^2|_{r=r_2}, \quad \sigma_r^2|_{r=r_3} = \sigma_r^3|_{r=r_3}, \quad \tau_{r\theta}^2|_{r=r_3} = \tau_{r\theta}^3|_{r=r_3}, \\ u_r^1|_{r=r_2} = u_r^2|_{r=r_2}, \quad u_\theta^1|_{r=r_2} = u_\theta^2|_{r=r_2}, \quad u_r^2|_{r=r_3} = u_r^3|_{r=r_3}, \quad u_\theta^2|_{r=r_3} = u_\theta^3|_{r=r_3}. \end{cases} \tag{40}$$

In addition, the inner surface of the casing is free of tractions, i.e.,

$$\sigma_r^1|_{r=r_1} = 0, \quad \tau_{r\theta}^1|_{r=r_1} = 0. \tag{41}$$

Substitution of Eqs. (31), (36), and (39) into Eqs. (40) and (41) gives rise to the following system of linear aligns:

$$\boldsymbol{M}\cdot\boldsymbol{X} = \boldsymbol{S}, \tag{42}$$

where $\boldsymbol{M}$ is a 10-by-10 matrix whose non-zero entries are given in Appendix A, and

$$\boldsymbol{X} = [A_1, B_1, C_1, D_1, A_2, B_2, C_2, D_2, C_3, D_3]^{\mathrm{T}},$$
$$\boldsymbol{S} = [0, 0, 0, 0, s, s, 0, 0, 0, 0]^{\mathrm{T}}.$$

From Eq. (42), the array $\boldsymbol{X}$ consisting of the unknown coefficients can be solved straightforwardly. Substitution of these coefficients back into Eqs. (31), (36), and (39) yields the stress and displacement distributions within the casing-cement-formation system as the solution of Sub-problem II.

2.4 Solution of complete problem and some remarks

In the previous subsections, stress and displacement solutions of the two sub-problems are obtained separately, and solutions of the complete problem can be obtained simply by superposition.

As mentioned in Section 1, some existing works have been devoted to similar topics as in this paper, i.e., analyzing the stress field within the casing-cement-formation system analytically, aiming at evaluating the mechanical integrity of the steel casing and the cement sheath[19,22,25–26]. However, these previous works have not included in-situ stresses in the formation as initial stresses in Hooke's law, and their displacement solutions are slightly different from those obtained in this paper.

Specifically, in Sub-problem I, their conditions in the formation are essentially

$$\sigma_\theta^0 = \sigma_r^0 = 0, \quad r_{\mathrm{i}} = r_3, \quad r_{\mathrm{o}} = \infty, \quad \sigma_{\mathrm{i}} = p_3, \quad \sigma_{\mathrm{o}} = \sigma, \tag{43}$$

which combining with Eq. (13) gives rise to the following radial displacement field within the formation:

$$u_r^3 = -\frac{\sigma}{\alpha_3} r + \frac{r_3^2(p_3 - \sigma)}{\beta_3} \frac{1}{r}. \tag{44}$$

Similarly, in the existing works, the conditions in the formation for Sub-problem II are

$$\sigma_r^0 = -\sigma_\theta^0 = 0, \quad \sigma_r|_{r=\infty} = -s\cos(2\theta), \quad \tau_{r\theta}|_{r=\infty} = s\sin(2\theta), \tag{45}$$

and therefore the displacement field within the formation is obtained as follows:

$$\begin{cases} u_r^3 = -\dfrac{1+\upsilon_3}{E_3}\Big(sr - (1-\upsilon_3)\dfrac{4C_3}{r} - \dfrac{2D_3}{r^3}\Big)\cos(2\theta), \\ u_\theta^3 = \dfrac{1+\upsilon_3}{2E_3}\Big(2sr - (1-2\upsilon_3)\dfrac{4C_3}{r} + \dfrac{4D_3}{r^3}\Big)\sin(2\theta). \end{cases} \tag{46}$$

Comparisons of Eq. (44) with Eq. (21) and Eq. (46) with Eq. (39) clearly show that additional displacements are predicted if the in-situ stresses in the formation are not included in Hooke's law as initial stresses.

For Sub-problem I, the additional radial displacement predicted by the existing method is

$$\delta u_r^3 = -\frac{\sigma}{\alpha_3} r, \tag{47}$$

while for Sub-problem II, the additional radial and tangential displacements are

$$\begin{cases} \delta u_r^3 = -\dfrac{1+\upsilon_3}{E_3} sr\cos(2\theta), \\ \delta u_\theta^3 = \dfrac{1+\upsilon_3}{E_3} sr\sin(2\theta). \end{cases} \tag{48}$$

Obviously, due to the requirement of displacement continuity at the cement-formation interface, these additional displacements in the formation will affect the stress distribution within the casing-cement-formation system, resulting in stress solutions different from those obtained with the present method.

It is our argument in this paper that these additional displacements in Eq. (47) and Eq. (48) predicted with the existing method have occurred along with the development of in-situ stresses in the formation during the sedimentary and tectonic processes, which should not be involved in the evaluation of the stress field in the casing-cement-formation system, since the casing and the cement have not taken part in the sedimentary and tectonic processes. During the oil/gas well construction and completion process, the rock mass within the well is removed and replaced by the steel casing and the cement sheath, and accordingly the support to the formation at the cement-formation interface changes from the original in-situ tractions to the final contact forces. It is this perturbation that causes displacements given in Eq. (21) and Eq. (39) in the formation near the wellbore, and results in the variation of the stress field in the formation from the in-situ stress state to the final one, as well as the development of stresses in the casing and the cement through displacement continuity at the casing-cement and the cement-formation interfaces. Therefore, inclusion of these additional displacements could result in inaccuracy in calculating the stresses in the casing-cement-formation system.

It is also possible to directly exclude these additional displacements by carefully examining Eqs. (44) and (46), or Eqs. (47) and (48). In these equations, it is noted that, as r increases, the additional displacements will increase linearly, leading to unbounded displacements in the far field away from the wellbore, which is apparently not realistic, since the displacements in the

far field due to the perturbation caused by well construction should vanish rather than increase with the increasing distance from the wellbore.

In summary, we have derived an analytical method for analyzing the stress distribution in the casing-cement-formation system which can serve as a basis for evaluating the integrity of the steel casing and the cement sheath. The new contribution here is that the unrealistic additional displacements in the formation, predicted by previous works, have been identified and excluded in present solutions via putting the in-situ stresses in the formation into Hooke's law as initial stresses. Some detailed analysis results will be provided in the following section to demonstrate the difference between the present method and the existing method.

3 Analysis results and discussion

In this section, validation of the present analytical method is given first by comparing analytical results with two-dimensional FEA results. This validation example also serves to introduce brief discussion on correct specification of proper boundary conditions in the FEA of geomechanical behavior of the near wellbore region of oil/gas wells. Subsequently, a series of sensitivity analysis results will be provided to illustrate the effect of elastic properties of the formation, cement, and the inner pressure of casing on the stress distribution within the casing and cement.

3.1 Validation of present analytical method

Consider an onshore vertical oil well drilled into a tight-oil reservoir located in the northwest of China. The depth of the production interval is approximately 3 400 m. The maximum horizontal principal stress σ_{H} is 82 MPa, while the minimum horizontal principal stress σ_{h} is 55 MPa. The internal pressure within the casing p_{w} is 34 MPa, which is representative of the hydrostatic pressure of a liquid at the target depth with a density of 1.0 g/cm^3. A 51/2-inch casing of P110 grade is installed and cemented in the 81/2-inch wellbore. The thickness of the casing is 10.54 mm. The geometric dimensions and the elastic properties of the casing, the cement, and the formation are given in detail in Table 1. Stresses within the casing-cement-formation system are evaluated using both the present analytical method and the existing analytical method.

Table 1 Geometric dimensions and elastic properties of casing-cement-formation system

Component	Young's modulus/GPa	Poisson's ratio	Inner radius/mm
Casing	210	0.30	59.31
Cement	12	0.25	69.85
Formation	10	0.20	107.95

Meanwhile, this validation example has also been analyzed using two FEA models shown in Fig. 3. In both models, the problem is simplified as a two-dimensional plane strain problem. In the first FEA model as shown in Fig. 3(a), in-situ stresses are applied at the boundaries as surface pressure loads, namely, the FEA-surface pressure, which is essentially equivalent to the existing analytical method in the sense of how the in-situ stresses are treated. In comparison, the second FEA model shown in Fig. 3(b) is slightly different, where the boundaries far away from the well are fixed in their normal directions, and the in-situ stresses are applied in the model as initial stresses in the rock formation. Therefore, the second FEA is called the FEA-initial stress. The second FEA model is equivalent to the present analytical method in the way of treating the in-situ stresses.

Figure 4 presents radial stress and hoop stress (or tangential stress) distributions along the 0° (σ_{H}) and 90° (σ_{h}) azimuths, obtained by the present analytical method and the existing analytical method as well as the two FEA models. Analytical results are plotted in solid lines

while FEA results are in dotted lines, and the two dashed lines separate the regions representing the casing, the cement, and the formation.

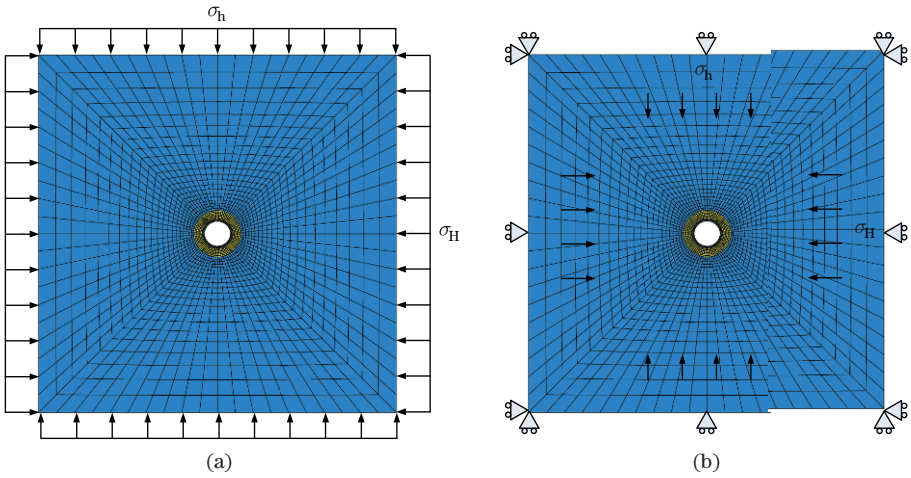

Fig. 3 Two finite element models for casing-cement-formation system, with in-situ stresses applied as (a) surface pressures on boundaries and (b) initial stresses in formation, respectively

It is clearly seen from Fig. 4 that results obtained by the present analytical method are in good agreement with those by the second FEA model where the in-situ stresses are applied as initial stresses, justifying the derivations of the present analytical method in this paper. Also, results from the existing analytical method coincide with those from the first FEA model with in-situ stress treated as surface pressures.

In Fig. 4, it is manifested that remarkable differences exist between the results obtained with the present analytical method and those obtained with the existing method. As shown in Fig. 4(a), the radial compressive stresses within the casing and the cement obtained with the present method are systematically less than those with the existing method, both in the 0° and 90° azimuths, and the differences in the cement are about 30 MPa. Similarly, it is noted from the inset of Fig. 4(b) that, within the cement, hoop compressive stresses with the present method are about 20 MPa to 30 MPa less than those with the existing method. In contrast, Fig. 4(b) shows that, in the casing, the hoop compressive stresses obtained with the present method are much less than those obtained with the existing method, especially in the 90° azimuth, where the difference can be more than 300 MPa. In addition, it can be observed from Fig. 4(b) that the difference of the hoop compressive stress in the 90° azimuth obtained with the present method and the existing method is larger than that in the 0° azimuth, which is caused by the stress concentration due to the fact that the horizontal in-situ stress σ_H in the 0° azimuth is larger than the horizontal in-situ stress σ_h in the 90° azimuth.

It is obvious that the existing analytical method overestimates the compressive stress level in the casing and cement sheath. As remarked in Subsection 2.4, the existing method does not include the in-situ stresses in Hook's law as initial stresses, resulting in additional displacements in the formation as shown in Eqs. (47) and (48). These additional displacements exert additional squeezing effects on the cement and the casing, leading to higher compressive stresses in the casing and the cement. Overestimation of the compressive stresses in the casing and the cement might be argued to be conservative when compressive or shear failure of the cement and collapse failure of the casing are of concern. However, if the burst failure of the casing or radial cracks within the cement is considered when the inner pressure of casing is increased as common in well testing and hydraulic fracturing jobs, overestimation of the hoop compressive stresses as exemplified in Fig. 4(b) might incur unexpected risks. In this regard, the present analytical method in this paper is superior to the existing method and gives more accurate results of the

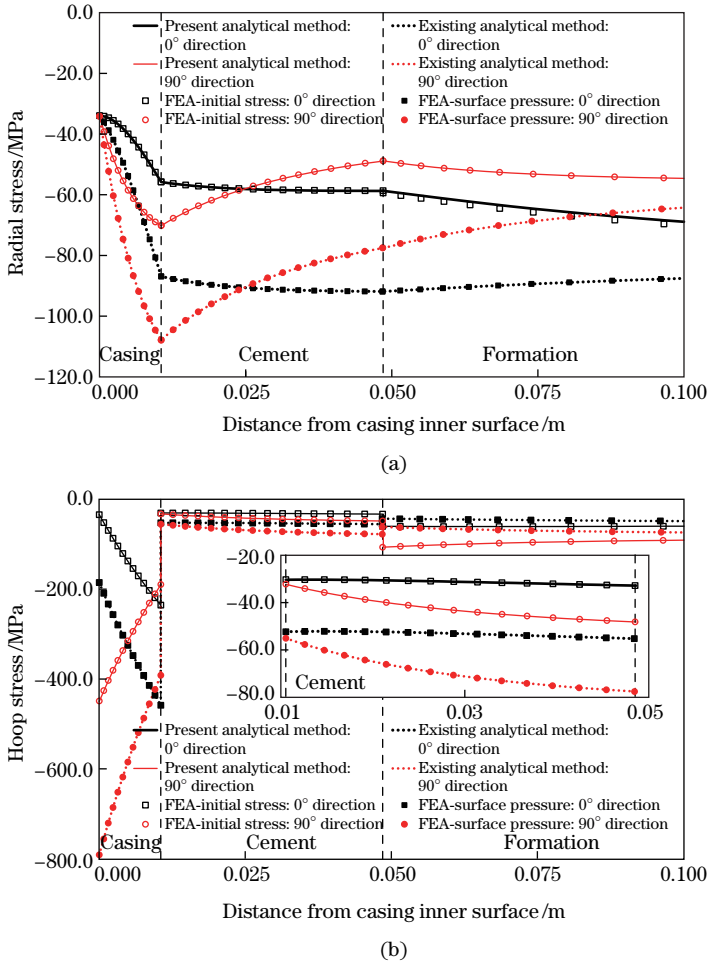

Fig. 4 (a) Radial stress and (b) hoop stress distribution in casing-cement-formation system along 0° (σ_H) and 90° (σ_h) azimuths varying with distance from casing inner wall, where inset in (b) is zoomed-in representation of hoop stress distribution in cement sheath

stress distributions within the casing-cement-formation system.

As an extra outcome of this validation example, here we would like to give some further remarks on the above two FEA models. Actually, in addition to the casing/cement integrity analysis, the FEA has already become a powerful tool in the analysis of geomechanical behavior of near wellbore regions, such as the wellbore stability analysis[28–29] and sand production analysis[30]. In existing literatures, both the two manners of treating the in-situ stresses shown in Fig. 3 have been used[9–10,12–15,28], and there seems no explicit discussion about which one is more reasonable. Here, in this paper, it is evident by Eqs. (47) and (48) and the results presented in this section that the frequently-adopted way of specifying boundary conditions in the FEA of near wellbore region as shown in Fig. 3(a) is not appropriate, since this will generate unrealistic additional displacements in the formation and thereby affects the stress distribution within the near wellbore region. A more appropriate way is to fix the boundaries at the far field of formation and apply the in-situ stresses as initial stresses, as shown in Fig. 3(b). A more comprehensive demonstration of this argument through various numerical analyses, such as wellbore stability analysis, sand production analysis, and cement/casing integrity analysis, is underway, and results will be published in a future publication.

3.2 Sensitivity analysis results

It has already been recognized in previous studies that mechanical properties of the cement and the formation have considerable effects on the stress distribution within the casing-cement-formation system. Here, we give the results of a series of sensitivity studies with the present analytical method, illustrating the effects of Young's moduli of the cement and the formation, Poisson's ratio of the cement, and the inner pressure of casing on the stress distribution within the casing and the cement. In obtaining the following results, the parameters in Table 1 are used except otherwise specified.

3.2.1 Effect of Young's modulus of formation

Figure 5 presents the radial stresses within the casing and the cement for formation elastic moduli of 2 GPa, 10 GPa, and 20 GPa. Results obtained with the present method are in solid lines, while those with the existing method are in dotted lines. Both results of the present method and those of the existing method show that, the lower Young's modulus of formation is, the higher compressive radial stresses within the casing and the cement are. This is easy to understand, since for softer rock formations, larger inward displacements will be generated under the same in-situ stresses, thus the squeezing effect on the cement and the casing from the formation is more notable, giving rise to higher compressive radial stresses within the casing and the cement. Similar to the observations in the validation example, compressive radial stresses calculated with the present method are lower than those with the existing method, and the lower Young's modulus of formation is, the larger the difference is. This is also can be explained by examining Eqs. (15), (47), and (48), which shows that the lower Young's modulus of formation is, the larger the additional displacements predicted with the existing method are, and thus the larger the compressive radial stresses overestimated with the existing method are.

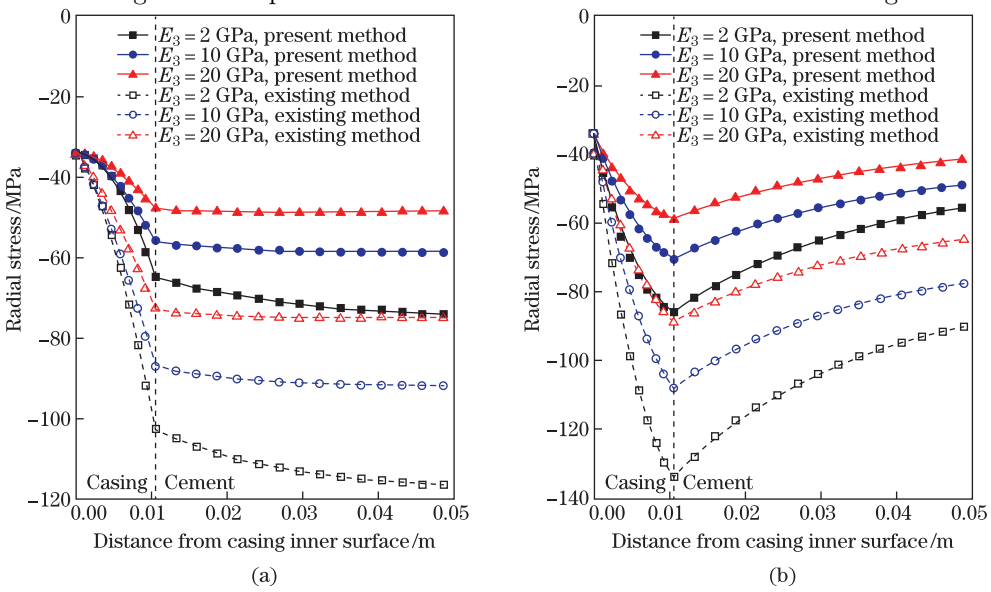

Fig. 5 Radial stress distributions in casing and cement along (a) 0° and (b) 90° azimuths varying with distance from casing inner wall for different Young's moduli of formation

Figure 6 shows the influence of Young's modulus of formation on the hoop stresses within the casing and the cement, from which it can be again observed that compressive hoop stresses within cement and the casing increase with decreasing Young's modulus of the formation. Also, it is manifested that the existing method overestimates the compressive hoop stresses within the casing and cement. For example, in Fig. 6(a), when $E_3 = 2$ GPa, the present method gives a tensile hoop stress on the casing inner wall in the 0° azimuth, indicating the expansion effect due to the inner pressure of casing overwhelms the squeezing effect of the formation, while the

existing method still predicts a compressive stress at the same location due to its overestimation of the squeezing effect.

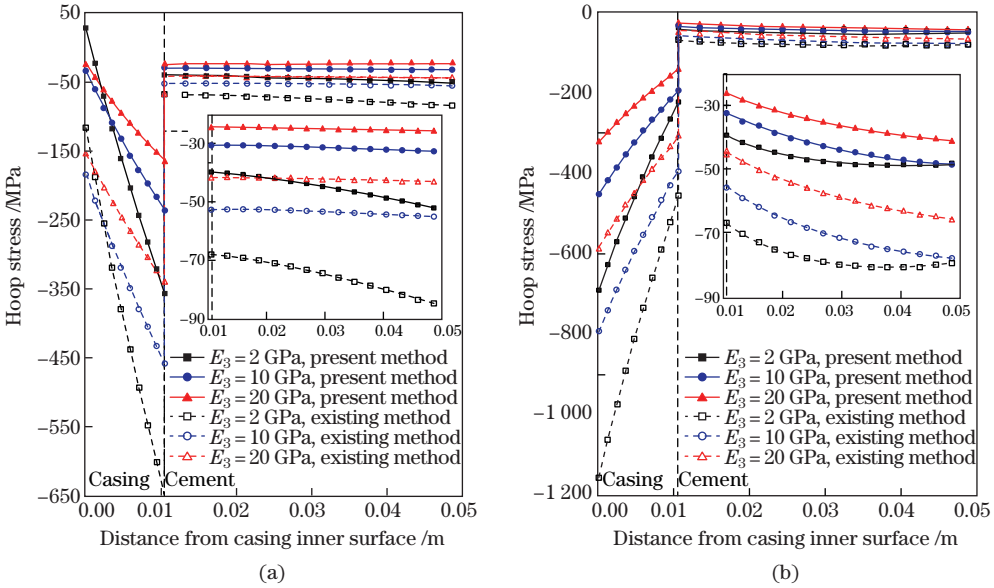

Fig. 6 Hoop stress distributions in casing and cement along (a) 0° and (b) 90° azimuths varying with distance from casing inner wall for different Young's moduli of formation, where insets are zoomed-in representations of hoop stresses in cement sheath

3.2.2 Effect of Young's modulus of cement

In Fig. 7, radial stresses within the casing and the cement for cement elastic moduli of 2 GPa, 10 GPa, and 20 GPa are given, while in Fig. 8, hoop stresses in the casing and the cement are provided. It is seen that, with decreasing Young's modulus of the cement, compressive radial and compressive hoop stresses within the casing and the cement decrease, while the tensile hoop

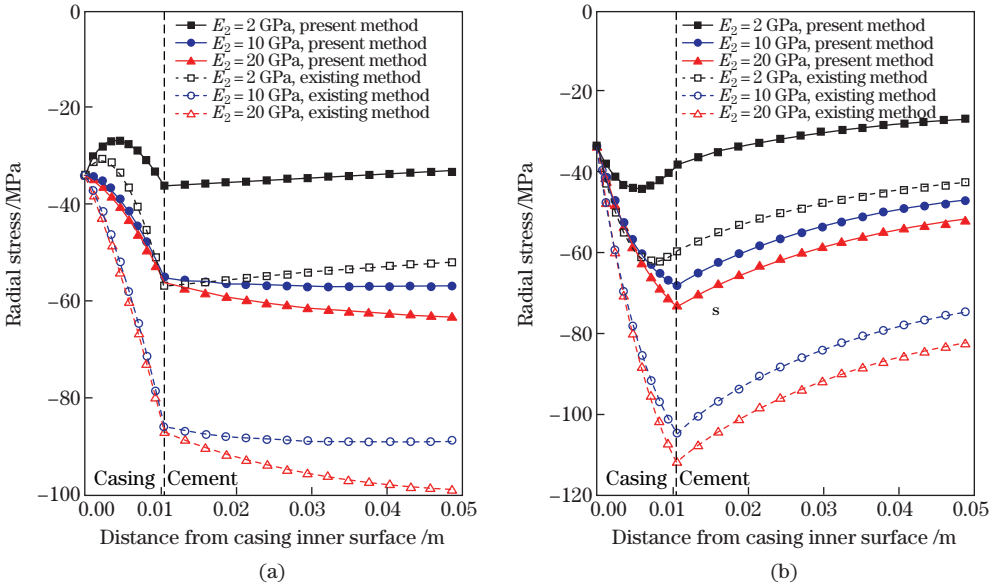

Fig. 7 Radial stress distributions in casing and cement along (a) 0° and (b) 90° azimuths varying with distance from casing inner wall for different Young's moduli of cement

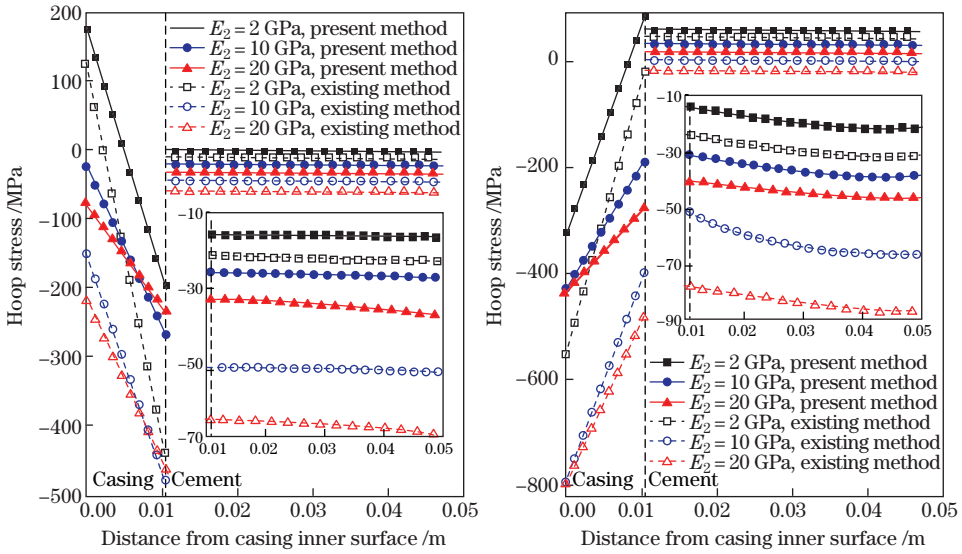

Fig. 8 Hoop stress distributions in casing and cement along (a) 0° and (b) 90° azimuths varying with distance from casing inner wall for different Young's moduli of cement, where insets are zoomed-in representations of hoop stresses in cement sheath

stresses at the inner wall of the casing in the 90° azimuth increase. Actually, the cement functions as a buffer layer between the formation and the casing. For the softer or more flexible cement, the inward displacement of the formation is more localized within the cement, which reduces the compressive stresses in the casing, while for the stiffer cement, the inward squeezing effect from the formation is more transmitted to the casing, and larger compressive stresses develop in the casing. In addition, lower cement Young's modulus also gives rise to lower compressive stresses in the cement.

Furthermore, it is evident that the difference between the results of the present method and those of the existing method also decreases with decreasing Young's modulus of the cement.

3.2.3 Effect of Poisson's ratio of cement

Radial stresses and hoop stresses within the casing and the cement for Poisson's ratio of cement of 0.10, 0.25, and 0.40 are given in Fig. 9 and Fig. 10, respectively. Results show that effects of Poisson's ratio of the cement on the stresses within the casing are not as large as the effects of Young's moduli of the formation and the cement as observed in previous subsections. On the other hand, compressive radial and compressive hoop stresses within the cement increase with increasing Poisson's ratio of the cement. Meanwhile, the compressive stresses within the cement overestimated with the existing method also increase with increasing Poisson's ratio of the cement.

3.2.4 Effect of inner pressure of casing

Scenarios with high inner pressure of casing are frequently encountered during the operating life circle of oil and gas wells, e.g., hydraulic fracturing, well testing, and high pressure flooding. A simple demonstration of the effect of the inner pressure of casing is shown in Fig. 11 and Fig. 12, where radial stresses and hoop stresses within the casing and the cement for inner pressures of casing of 34 MPa and 70 MPa are presented, respectively. In Fig. 11, it can be seen that, for either softer cement (E_2 = 2 GPa) or stiffer cement (E_2 = 20 GPa), the higher inner pressure of casing generates higher compressive radial stresses within the casing and the cement. In Fig. 12, with the increasing inner pressure of casing, tensile hoop stresses in the casing increase while compressive hoop stresses decrease. For the stiffer cement (E_2 =

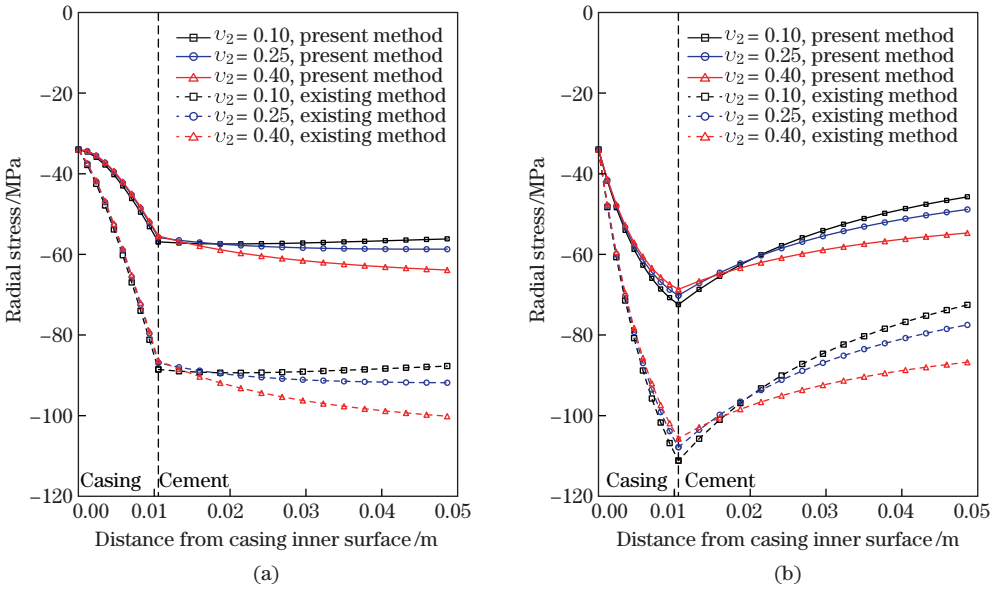

Fig. 9 Radial stress distributions in casing and cement along (a) 0° and (b) 90° azimuths varying with distance from casing inner wall for different Poisson's ratios of cement

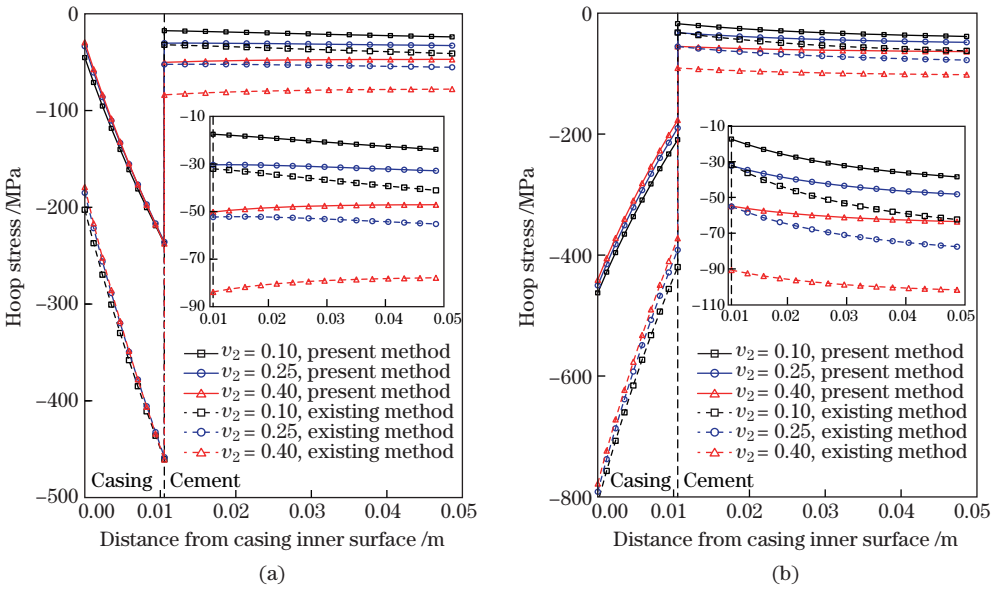

Fig. 10 Hoop stress distributions in casing and cement along (a) 0° and (b) 90° azimuths varying with distance from casing inner wall for different Poisson's ratios of formation, where insets are zoomed-in representations of hoop stresses in cement sheath

20 GPa), compressive hoop stresses within the cement decrease with the increasing inner pressure of casing. However, for the softer cement (E_2 = 2 GPa), the hoop stresses within the cement are almost not influenced by the inner pressure of casing. It seems that the softer cement is more insensitive to the pressure variation in the casing, indicating the soft or flexible cement is likely to endure the high inner pressure of casing during operations like hydraulic fracturing and high pressure flooding, as also noticed by Thiercelin et al.[21].

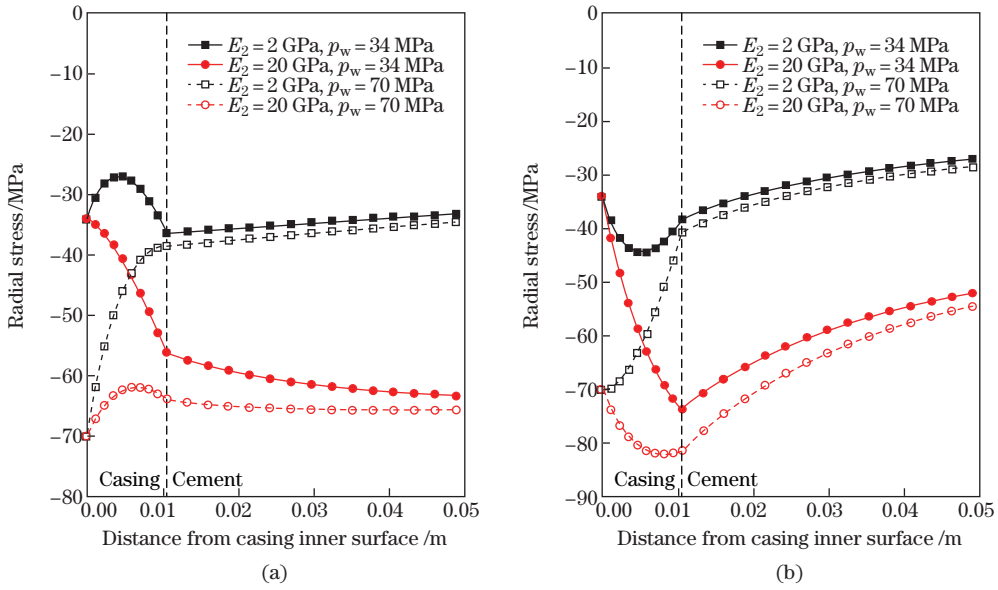

Fig. 11 Radial stress distributions in casing and cement along (a) 0° and (b) 90° azimuths varying with distance from casing inner wall for different inner pressures of casing

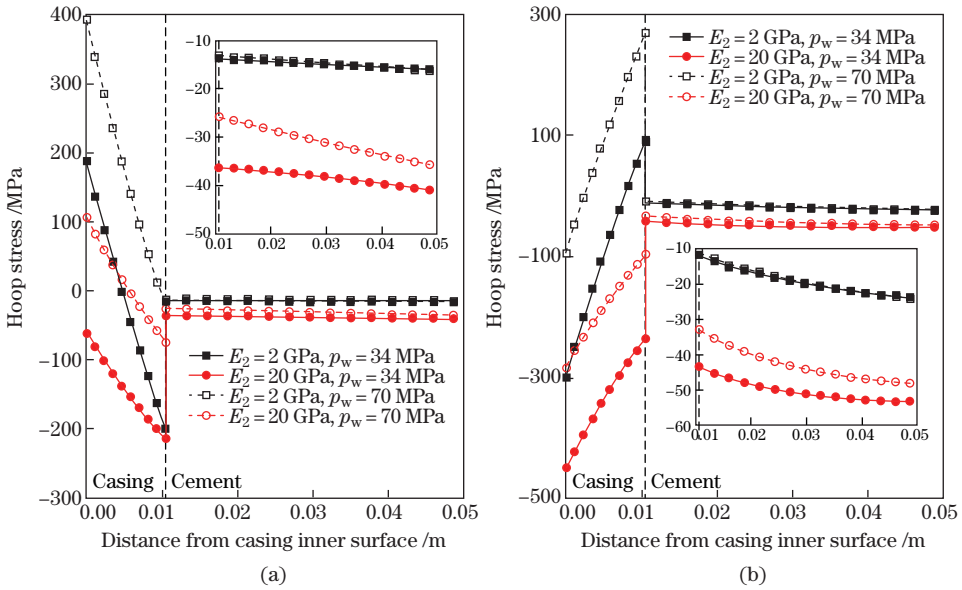

Fig. 12 Hoop stress distributions in casing and cement along (a) 0° and (b) 90° azimuths varying with distance from casing inner wall for different inner pressures of casing, where insets are zoomed-in representations of hoop stresses in cement sheath

4 Conclusions

Determination of the stress field within the steel casing and the cement sheath of the oil/gas well is of fundamental importance for engineering designs that are aimed at ensuring the integrity of the casing and the cement during the whole operating life of oil/gas wells. In this paper, a revised analytical method has been proposed for evaluating the stresses within the

casing-cement-formation system under combined application of anisotropic horizontal in-situ stresses in the formation and uniform pressure on the casing inner wall. The problem is divided into two sub-problems. The first sub-problem is to solve the stress field within the casing-cement-formation system under uniform horizontal in-situ stresses in the formation and uniform inner pressure on the casing inner wall, while in the second sub-problem, only deviatoric in-situ stresses exist in the formation, and the casing inner wall is traction-free. The solution of the complete problem is obtained by superposing the solutions of the two sub-problems.

The new contribution in this paper is that, by treating the in-situ stresses as initial stresses in the formation, we exclude the unrealistic additional displacements within the formation predicted with the existing method. Therefore, we can more realistically describe the squeezing effect from the formation, and more accurately evaluate the stresses within the casing-cement-formation system. Actually, in-situ stresses within the formation have already arisen during the sedimentary and tectonic processes when the cement sheath and the steel casing are not present. Placement of the casing and the cement sheath into the well perturbs the stress state within the formation, from in-situ stresses to final stresses. It is this perturbation that generates inward displacements within the formation, and thus the in-situ stress state should be taken as a starting point, which justifies the requirement of treating the in-situ stresses as initial stresses as proposed in the present method. Results of the validation example in Subsection 3.1 demonstrate that the existing method overestimates the compressive stress level in the casing and the cement sheath, while the present method would give more accurate results.

Through a series of sensitivity analyses, effects of Young's moduli of the formation and the cement, Poisson's ratio of the cement, and the inner pressure of casing on the stresses in the casing and the cement are illustrated. It is shown that the compressive radial and hoop stresses within the casing and the cement increase with the decreasing modulus of the formation, or increasing modulus of the cement. It is also evident that influence of Poisson's ratio of the cement on the stresses within the casing is not as large as the influence of Young's moduli of the formation and the cement, while compressive radial and hoop stresses within the cement increase with increasing Poisson's ratio of the cement. In addition, results indicate that the soft or flexible cement is likely to endure the high inner pressure of casing due to its insensitivity of the inner pressure variation of casing.

Finally, it is worth mentioning that the present method should be viewed as an attempt to revise the existing method by appropriately applying in-situ stresses in the formation. For future improvement of the present method, factors like the evolution of cement properties during the setting process, the chemical shrinkage or expansion of the cement and the poroelastic effect of the formation that would complicate the stress field are needed to be incorporated.

References

[1] Vignes, B. and Aadnøy, B. S. Well-integrity issues offshore norway. *SPE Production and Operations*, **25**, 145–150 (2010)

[2] Boukhelifa, L., Moroni, N., James, S. G., Le Roy-Delage, S., Thiercelin, M. J., and Lemaire, G. Evaluation of cement systems for oil-and gas-well zonal isolation in a full-scale annular geometry. *SPE Drilling and Completion*, **20**, 44–53 (2005)

[3] Li, Z., Zhang, K., Guo, X., Liu, J., Cheng, X., and Du, J. Study of the failure mechanisms of a cement sheath based on an equivalent physical experiment. *Journal of Natural Gas Science and Engineering*, **31**, 331–339 (2016)

[4] Bois, A. P., Garnier, A., Galdiolo, G., and Laudet, J. B. Use of a mechanistic model to forecast cement-sheath integrity. *SPE Drilling and Completion*, **27**, 303–314 (2012)

[5] Bai, M., Sun, J., Song, K., Reinicke, K. M., and Teodoriu, C. Evaluation of mechanical well integrity during CO_2 underground storage. *Environmental Earth Sciences*, **73**, 6815–6825 (2015)

[6] Bellabarba, M., Bulte-Loyer, H., Froelich, B., Le Roy-Delage, S., van Kuijk, R., Zeroug, S., Guillot, D., Moroni, N., Pastor, S., and Zanchi, A. Ensuring zonal isolation beyond the life of the well. *Oilfield Review*, **20**, 18–31 (2008)

[7] Dusseault, M. and Jackson, R. Seepage pathway assessment for natural gas to shallow groundwater during well stimulation, in production, and after abandonment. *Environmental Geosciences*, **21**, 107–126 (2014)

[8] Goodwin, K. J. and Crook, R. J. Cement sheath stress failure. *SPE Drilling Engineering*, **7**, 291–296 (1992)

[9] Fleckenstein, W. W., Eustes, A. W., III, and Miller, M. G. Burst-induced stresses in cemented wellbores. *SPE Drilling and Completion*, **16**, 74–82 (2011)

[10] Nabipour, A., Joodi, B., and Sarmadivaleh, M. Finite element simulation of downhole stresses in deep gas wells cements. *SPE Deep Gas Conference and Exhibition*, Society of Petroleum Engineerings, Manama, 1–13 (2010)

[11] Philippacopoulos, A. J. and Berndt, M. L. Structural analysis of geothermal well cements. *Geothermics*, **31**, 657–676 (2002)

[12] Wong, R. C. K. and Yeung, K. C. Structural integrity of casing and cement annulus in a thermal well under steam stimulation. *Journal of Canadian Petroleum Technology*, **45**, 6–9 (2006)

[13] Ravi, K., Bosma, M., and Gastebled, O. Improve the economics of oil and gas wells by reducing the risk of cement failure. *IADC/SPE Drilling Conference*, Society of Petroleum Engineerings, Dallas, 1–13 (2002)

[14] Bosma, M., Ravi, K., van Driel, W., and Schreppers, G. J. Design approach to sealant selection for the life of the well. *SPE Annual Technical Conference*, Society of Petroleum Engineerings, Houston, 1–14 (1999)

[15] Gray, K. E., Podnos, E., and Becker, E. Finite-element studies of near-wellbore region during cementing operations: part I. *SPE Drilling and Completion*, **24**, 127–136 (2009)

[16] Salehabadi, M., Jin, M., Yang, J., Haghighi, H., Ahmed, R., and Tohidi, B. Finite element modeling of casing in gas-hydrate-bearing sediments. *SPE Drilling and Completion*, **24**, 545–552 (2009)

[17] Shahri, M., Schubert, J. J., and Amani, M. Detecting and modeling cement failure in high-pressure/high-temperature (HP/HT) wells using finite element method (FEM). *International Petroleum Technology Conference*, Society of Petroleum Engineerings, Doha, 1–10 (2005)

[18] Shen, Z. and Beck, F. E. Three-dimensional modeling of casing and cement sheath behavior in layered, nonhomogeneous formations. *IADC/SPE Asia Pacific Drilling Technology Conference and Exhibition*, Society of Petroleum Engineerings, Tianjin, 1–10 (2012)

[19] Atkinson, C. and Eftaxiopoulos, D. A plane model for the stress field around an inclined, cased and cemented wellbore. *International Journal for Numerical and Analytical Methods in Geomechanics*, **20**, 549–569 (1996)

[20] Yuan, Z., Gardoni, P., Schubert, J., and Teodoriu, C. Cement failure probability analysis in water injection well. *Journal of Petroleum Science and Engineering*, **107**, 45–49 (2013)

[21] Thiercelin, M. J., Dargaud, B., Baret, J. F., and Rodriquez, W. J. Cement design based on cement mechanical response. *SPE Drilling and Completion*, **13**, 266–273 (1998)

[22] Yin, Y. Q., Chen, Z. W., and Li, P. E. Theoretical solutions of stress distribution in casing-cement and stratum system (in Chinese). *Aata Mechanica Sinica*, **38**, 835–842 (2006)

[23] Li, B., Guo, B., Li, H., and Shi, Y. An analytical solution to simulate the effect of cement/formation stiffness on well integrity evaluation in carbon sequestration projects. *Journal of Natural Gas Science and Engineering*, **27**, 1092–1099 (2015)

[24] Li, Y., Liu, S., Wang, Z., Yuan, J., and Qi, F. Analysis of cement sheath coupling effects of temperature and pressure in non-uniform in-situ stress field. *International Oil and Gas Conference and Exhibition in China*, Society of Petroleum Engineerings, Tianjin, 1–8 (2010)

[25] Wang, Y. B., Gao, D. L., and Fang, J. Assessment of wellbore integrity of offshore drilling in well testing and production. *Journal of Engineering Mechanics*, **142**, 04016030 (2016)

[26] Zhang, L., Yan, X., Yang, X., and Zhao, X. Evaluation of wellbore integrity for HTHP gas wells under solid-temperature coupling using a new analytical model. *Journal of Natural Gas Science and Engineering*, **25**, 347–358 (2015)

[27] Timoshenko, S. and Goodier, J. *Theory of Elasticity*, McGraw-Hill, New York, 55–81 (1951)

[28] Papanastasiou, P. C. and Vardoulakis, I. G. Numerical treatment of progressive localization in relation to borehole stability. *International Journal for Numerical and Analytical Methods in Geomechanics*, **16**, 389–424 (1992)

[29] Salehi, S., Hareland, G., and Nygaard, R. Numerical simulations of wellbore stability in under-balanced-drilling wells. *Journal of Petroleum Science and Engineering*, **72**, 229–235 (2010)

[30] Volonte, G., Scarfato, F., and Brignoli, M. Sand prediction: a practical finite-element 3D approach for real field applications. *SPE Production and Operations*, **28**, 95–108 (2013)

Appendix A

Non-zero entries of the 10-by-10 matrix M in Eq. (42) are given as

$$M_{12}=1,\quad M_{13}=2/r_1^2,\quad M_{14}=3/r_1^4,$$

$$M_{21}=3r_1^2,\quad M_{22}=1,\quad M_{23}=-1/r_1^2,$$

$$M_{24}=-3/r_1^4,\quad M_{32}=1,\quad M_{33}=2/r_2^2,$$

$$M_{34}=3/r_2^4,\quad M_{35}=-1,\quad M_{36}=-2/r_2^2,$$

$$M_{37}=-3/r_2^4,\quad M_{41}=3r_2^2,\quad M_{42}=1,$$

$$M_{43}=-1/r_2^2,\quad M_{44}=-3/r_2^4,\quad M_{45}=-3r_2^2,$$

$$M_{46}=-1,\quad M_{47}=1/r_2^2,\quad M_{48}=3/r_2^4,$$

$$M_{56}=1,\quad M_{57}=2/r_3^2,\quad M_{58}=3/r_3^4,$$

$$M_{59}=-2/r_3^2,\quad M_{5,10}=-3/r_3^4,\quad M_{65}=3r_3^2,$$

$$M_{66}=1,\quad M_{67}=-1/r_3^2,\quad M_{68}=-3/r_3^4,$$

$$M_{69}=1/r_3^2,\quad M_{6,10}=3/r_3^4,\quad M_{71}=2\upsilon_1 r_2^3/G_1,$$

$$M_{72}=r_2/G_1,\quad M_{73}=-2(1-\upsilon_1)/(G_1 r_2),$$

$$M_{74}=-1/(G_1 r_2^3),\quad M_{75}=-2\upsilon_2 r_2^3/G_2,$$

$$M_{76}=-r_2/G_2,\quad M_{77}=2(1-\upsilon_2)/(G_2 r_2),$$

$$M_{78}=1/(G_2 r_2^3),\quad M_{81}=(3-2\upsilon_1)r_2^3/G_1,$$

$$M_{82}=r_2/G_1,\quad M_{83}=-(1-2\upsilon_1)/(G_1 r_2),$$

$$M_{84}=1/(G_1 r_2^3),\quad M_{85}=-(3-2\upsilon_2)r_2^3/G_2,$$

$$M_{86}=-r_2/G_2,\quad M_{87}=(1-2\upsilon_2)/(G_2 r_2),$$

$$M_{88}=-1/(G_2 r_2^3),\quad M_{95}=2\upsilon_2 r_3^3/G_2,$$

$$M_{96} = r_2/G_2, \quad M_{97} = -2(1-\upsilon_2)/(G_2 r_3),$$

$$M_{98} = -1/(G_2 r_3^3), \quad M_{99} = 2(1-\upsilon_3)/(G_3 r_3),$$

$$M_{9,10} = 1/(G_3 r_3^3), \quad M_{10,5} = (3-2\upsilon_2) r_3^3/G_2,$$

$$M_{10,6} = r_3/G_2, \quad M_{10,7} = 2(1-\upsilon_3)/(G_3 r_3),$$

$$M_{10,8} = 1/(G_3 r_3^3), \quad M_{10,9} = (1-2\upsilon_3)/(G_3 r_3),$$

$$M_{10,10} = -1/(G_3 r_3^3),$$

where G_1, G_2, and G_3 are shear moduli of the casing, the cement, and the formation, respectively, and

$$G_i = \frac{E_i}{2(1+\upsilon_i)}, \quad i = 1, 2, 3.$$